Synthesis and Characterizations of Amorphous Carbon Nanotubes by Pyrolysis of Ferrocene Confined within AAM Templates

ARTICLE *in* THE JOURNAL OF PHYSICAL CHEMISTRY B · MAY 2006

Impact Factor: 3.3 · DOI: 10.1021/jp0568475 · Source: PubMed

5 AUTHORS, INCLUDING:

Qing Chen
Peking University
172 PUBLICATIONS **5,979** CITATIONS
SEE PROFILE

Lian-Mao Peng
Peking University
394 PUBLICATIONS **9,696** CITATIONS
SEE PROFILE

THE JOURNAL OF PHYSICAL CHEMISTRY B

Article

Synthesis and Characterizations of Amorphous Carbon Nanotubes by Pyrolysis of Ferrocene Confined within AAM Templates

Z. D. Hu, Y. F. Hu, Q. Chen, X. F. Duan, and L.-M. Peng

J. Phys. Chem. B, **2006**, 110 (16), 8263-8267• DOI: 10.1021/jp0568475 • Publication Date (Web): 05 April 2006

Synthesis and Characterizations of Amorphous Carbon Nanotubes by Pyrolysis of Ferrocene Confined within AAM Templates

Z. D. Hu,[†] Y. F. Hu,[‡] Q. Chen,[‡] X. F. Duan,[†] and L.-M. Peng*,[‡]

Key Laboratory for the Physics and Chemistry of Nanodevices and Department of Electronics, Peking University, Bejing 100871, China, and National Center for Condensed Matter Physics, Institute of Physics, Chinese Academy of Science, P.O. Box 603, Beijing 100080, China

Received: November 25, 2005; In Final Form: February 23, 2006

Amorphous carbon nanotubes (a-CNTs) are synthesized by pyrolysis of ferrocene confined in the nanopores of the anodic alumina membrane (AAM) and characterized by field emission scanning electron microscopy (SEM), energy-dispersive X-ray spectroscopy (EDS), transmission electron microscopy (TEM), electron energy-loss spectroscopy (EELS), and Raman spectroscopy. It is shown that the a-CNT has an ultrathin amorphous wall (∼3 nm) and a relatively large diameter (∼50 nm), and is capsulated with iron oxide nanoparticles. It is found that the growth of the a-CNTs is governed mainly by the template limitation effect. Electrical transport measurements on individual a-CNTs demonstrate that the a-CNT may be connected with electrodes via either ohmic or Schottky contacts, and the resisitivity of the a-CNTs was measured to be 4.5×10^{-3} Ω cm.

1. Introduction

Recently nanostructured materials have stimulated a great interest due to their unique electrical and optical properties endowed by the exotic density of states distribution characteristic of low-dimensional systems. Carbon nanotubes (CNTs), first discovered by Iijima in 1991,[1] were intensively investigated for their striking properties and potential to impact broad areas of science and technology.[2] So far numerous methods have been developed for the synthesis of CNTs, such as arc discharge,[3] laser ablation,[4] and chemical vapor deposition (CVD).[5] Early works focused mainly on "ideal" carbon nanotubes with perfect concentric graphene shells. However, defects such as pentagons, heptagons, vacancies, and impurities are inevitably present in the well-prepared CNTs. The introduction of defects in the carbon network can lead to interesting properties and new potential nanodevices.[6] Rakitin et al.[7] investigated both theoretically and experimentally the nanotubes comprised mainly of disordered graphene and found that this type of nanotube displayed a semiconductor band gap that is inversely proportional to the diameter and larger than corresponding crystalline tubes. The chirality problem is absent in the amorphous CNTs (a-CNTs), which is favorable to certain applications such as in some nanoelectronics and sensor devices. Thereafter various methods were developed to produce amorphous CNTs.[8−11]

The template method was proved to be a superb approach to the preparation of nanomaterials, including CNTs.[12,13] Herein we report a template method for the synthesis of amorphous CNTs, in combination with the closed space sublimation (CSS) technique, which has been used to prepare single crystalline semiconductor nanowires.[14] Two stages are involved in our experiment: sublimation of ferrocene into the nanopores of the template and pyrolysis of the confined ferrocene under an argon atmosphere. This CSS-assisted method of synthesis differs from that reported in the literature[12,24,25] in that the precursor was introduced into the nanochannels first and then pyrolyzed in the confined space. The resulting products are tubular structures with amorphous ultrathin wall and iron oxide nanoparticles encapsulated. The limited supply of carbonaceous precursor results in the ultrathin wall. Nanoelectronic devices were fabricated by using the a-CNTs and their electrical properties were investigated.

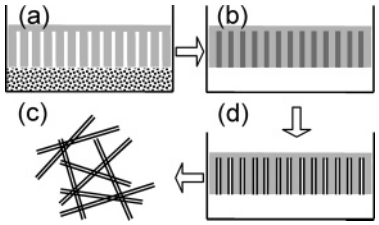

Figure 1. Schematic diagrams showing the process of synthesizing a-CNTs.

2. Experimental Section

The synthesis routine is schematically shown in Figure 1. Anodic alumina membrane (AAM) templates were prepared by a conventional two-step anodization process.[15] The free-standing template was placed with its opening end facing down toward a 10 mL alumina crucible containing 1 g of ferrocene powder (A. R. grade), as shown in Figure 1a. The crucible was then transferred into the center of a quartz tube inserted in a horizontal tube furnace. The tube was pumped by employing a mechanical pump and refilled with high-purity argon (99.999%) for several cycles to eliminate residue oxygen. Subsequently, the furnace was ramped uniformly to 150 °C and held at this temperature for 60 min. The furnace temperature was then rapidly increased to 750 °C and held at that temperature for 30 min. Finally, the system was allowed to cool to room temperature. A constant flow (50 mL/min) of high-purity Ar was passed through the quartz tube during the whole process. The template transformed from transparent to black. Then the AAM template

* Author to whom correspondence should be addressed. E-mail: lmpeng@pku.edu.cn.
[†] Chinese Academy of Science.
[‡] Peking University.

10.1021/jp0568475 CCC: $33.50
Published on Web 04/05/2006

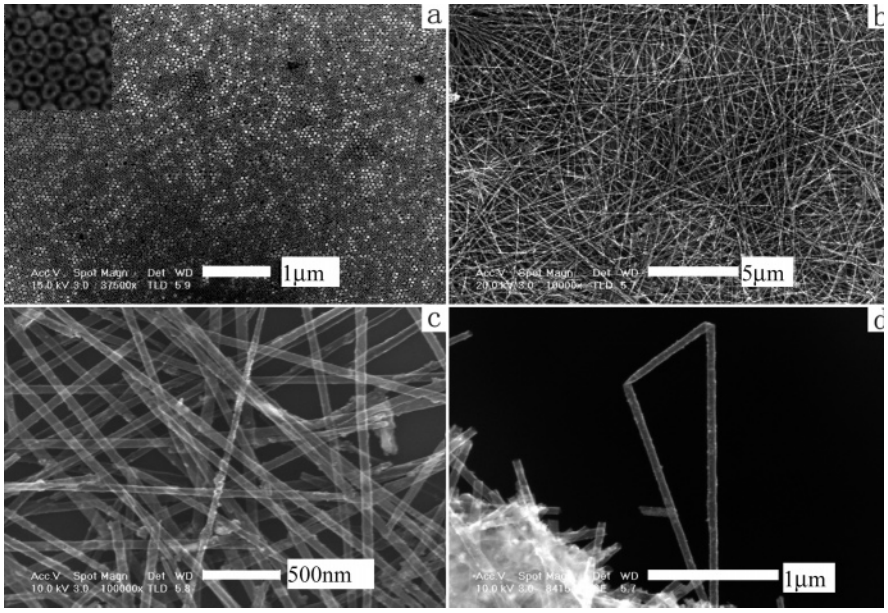

Figure 2. Typical SEM images of the a-CNTs: (a) a top view of an AAM template embedded with a-CNTs (the inset in part a shows an enlarged image); (b) dispersed a-CNTs on a Si wafer; (c) a magnified image of part b; and (d) a bent a-CNT illustrating its rigidity.

embedded with CNTs was immersed into a 6 M aqueous NaOH solution for about 2 h to completely remove the alumina. After filtration utilizing a vacuum pump filter, the products were dried at 50 °C for 20 min.

The as-prepared CNTs were characterized and analyzed by a Philips XL30-S-FEG scanning electron microscopy (SEM), energy-dispersive X-ray spectroscopy (EDS), transmission electron microscopy (TEM) with a Philips CM200 equipped with a Gatan Imaging Filtering (GIF) system at 200 kV, and electron energy-loss spectroscopy (EELS). The energy dispersion was set to be 0.1 eV/channel and the spectrum was collected in the image mode. The Raman spectrum was recorded with a JY-T64000 spectrometry system ranging from 700 to 2000 cm^{-1} at room temperature. The 532 nm line of an Ar ion laser was used for excitation, with an output power of 1.5 mW.

CNTs were dispersed in ethanol and dropped onto a SiO_2 substrate. Electron beam lithography, metal deposition, and lift-off were used to form contacts with individual CNTs. Two different electrodes were fabricated on the top of the CNT, i.e., 30 nm Au and 15 nm Ti/5 nm Au. Electrical transport measurements were carried out in a vacuum with a Keithley 4200 semiconductor characterization system with preamplifer.

3. Results and Discussions

We first characterized the samples using a FEG-SEM. Shown in Figure 2a is a top view of the AAM template. This image shows clearly that highly ordered and closely packed nanotubes with their open tips were embedded in the AAM template (see the insert of Figure 2a). After complete removal of the template and filtration, the resultant products looked like a sheet of carbon paper. Figure 2b shows CNTs dispersed on a Si wafer, and Figure 2c shows a magnified image of these CNTs. It is noted that the nanotubes look almost transparent in SEM observations with an acceleration voltage of 10 kV, suggesting that the wall thickness of the nanotubes is very thin. The surface of the wall is smooth and no absorbed clusters were observed. In addition, the nanotubes seem more rigid, compared with well-graphitized CNTs produced by other methods. Figure 2d illustrates a bent nanotube, featuring the inflexibility of the nanotubes. One possible reason for the observed rigidity results from the mixture

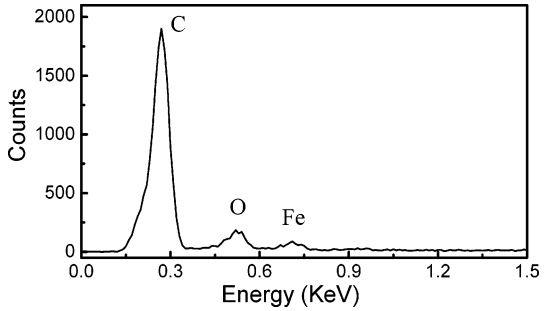

Figure 3. Energy-dispersive X-ray spectrum taken from a-CNT sample, suggesting that the sample is composed mainly of carbon plus a small amount of iron oxide.

of the carbon sp^3 and sp^2 hybridization, as confirmed by the subsequent EELS analysis. The sample composition was identified by EDS analysis (Figure 3). Apart from the carbon and iron peaks, the oxygen peak is also detected. The oxygen was presumably introduced by the residue oxygen absorbed on the wall of the tubes and leakage that might further react with iron to form iron oxide.

TEM and high-resolution TEM (HRTEM) observations were carried out in order to elucidate the structure of the CNTs. Figure 4a is a low-magnification TEM image of CNTs, revealing that the CNTs are straight nanotubes with an average diameter of ~50 nm, and this value is consistent with the corresponding nanopore size of the AAM template we used. Figure 4a also shows that the CNT has an open end.

Many dark nanoparticles distributed within the nanotubes are observed. HRTEM (Figure 4b) in combination with EDS analysis shows that these particles are crystalline iron oxide nanoparticles (4−8 nm) with a round or faceted morphology. They are either coated with amorphous carbon shell or naked. The wall thickness of the CNTs is only ~3 nm compared with its large diameter, which is much thinner than the result reported in ref 13.

EELS can be used to determine the nature of the C bonding. Representative EELS results on the a-CNT sample are presented in Figure 5, showing clearly two energy loss peaks. The first narrow peak around 285 eV corresponds to transitions from carbon 1s to the antibonding π^* states, characteristic of the sp^2-

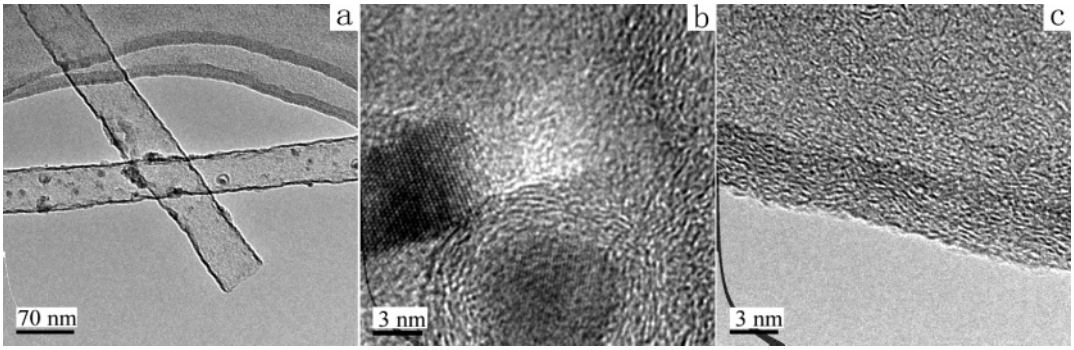

Figure 4. TEM and HRTEM images of a-CNTs: (a) representative TEM micrograph of a-CNTs; (b) HRTEM image of a nanotube encapsulated with iron oxide nanoparticles (the particle is bare or enwrapped by an amorphous carbon shell); and (c) HRTEM image showing the ultrathin amorphous wall.

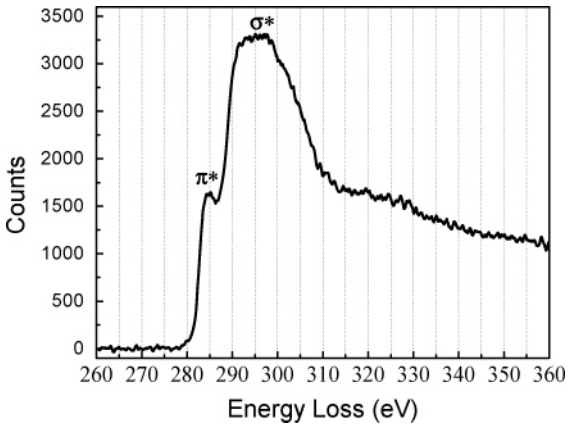

Figure 5. Eelectron energy loss spectrum of the C edge of an a-CNT.

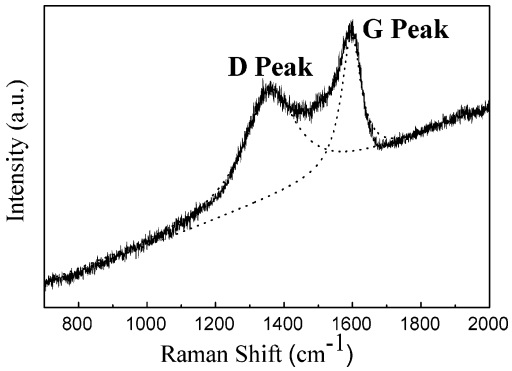

Figure 6. A typical Raman spectrum (532 nm excitation) from the a-CNT sample showing the G peak (1596 cm^{-1}) and D peak (1361 cm^{-1}). The curves were fitted with Gaussian line shapes.

bonded carbon, while the broader peak at 290−310 eV indicates transition to the antibonding σ^* states associated with the sp^3-bonded carbon. The amorphous microstructure is essentially segregated sp^2 clusters embedded in a sp^3-bonded matrix. π bonds are weaker than σ bonds but they govern the electronic properties of the amorphous carbon structure such as their optical gap, whereas σ bonds determine their mechanical properties such as hardness. π bonds are present mainly in sp^2 hybrids. It is expected that the tetrahedral disposition of σ bonds in sp^3 hybrids contributes to the hardness of the amorphous carbon wall much more than the sp^2 hybrids.

The amorphous nature of the a-CNTs is further investigated by Raman spectroscopy, as shown in Figure 6. The spectrum exhibits two prominent peaks, i.e., D peak (1361 cm^{-1}) and G peak (1596 cm^{-1}), which were fitted with two Gaussian line shapes. The G peak corresponds to the high-frequency Raman active E_{2g} mode of graphite. Compared with the G-band at 1580 cm^{-1} for the graphitic carbons, the G-band of the nanotubes shifts toward a higher wavenumber indicating the existence of nanocrystalline graphite or sp^2 clusters.[16] The strong and broad D peak (A_{1g} mode) was attributed to disorder-induced carbon features arising from finite particle size or lattice distortion. The intensity ratio between D and G peaks can be used to evaluate the graphitization of carbon materials. This ratio is inversely proportional to the degree of graphitization. As shown in Figure 6, the value is 0.8, manifesting a low degree of graphitization in the as-prepared CNTs. The modes of sp^3 bonding in nanotubes tend not to show up in the Raman spectrum, because visible Raman spectroscopy is 50−230 times more sensitive to sp^2 sites than to sp^3. Visible photons preferentially excite electrons to π^* states.[16]

The formation process of the a-CNTs is depicted in Figure 1 and it consists of four steps.

Step 1: An alumina crucible containing powdery ferrocene and an AAM template was transferred into the quartz tube.

Step 2: Ferrocene powder was sublimated into the nanochannels of the AAM template at Ar ambient. Ferrocene ($Fe(C_5H_5)_2$, abbreviated $FeCp_2$) is thermally stable below 500 °C. When the temperature was raised to above 100 °C, it began to sublimate.[17] After a 60-min period of sublimation no ferrocene powder remained in the crucible. Thus the ferrocene filled within the AAM pores was the only carbon source for the subsequent CNT growth.

Step 3: Pyrolyzing ferrocene at 750 °C led to a-CNT formation. Theoretical calculation with density functional theory[18] revealed that binding energies of a ferrocene molecule are 1480 kJ/mol for the Fe−Cp bond, 602 kJ/mol for the C−C bond, and 492 kJ/mol for C−H bond. Further molecule dynamics simulation at 1000 K[18] showed that the hydrogen atoms leave the ferrocene first, and then the cyclopentadienyl ring started to break up, followed by the breakage of the Fe−C bonds in combination with the remaining C−C bonds. Hence the decomposition products emerged in the following sequence: H, C−H, C, C_2, C_3, and finally Fe. Although in our experiment ferrocene started to decompose below 1000 K, we believe that it followed basically the same decomposition sequence (although the confinement within nanometer scale pores may alter the exact decomposition temperature, etc.). During the pyrolysis process, most of the resulting H escaped in the form of H_2 because of the long period of heat treatment, while a bit of H still stayed in the carbon to saturate carbon-dangling bonds. The C−H and C clusters (C, C_2, and C_3) reacted with each other and readily absorbed on the inner wall of the nanopores to build up tubular structures. Martin[17] reported that the inner surface of the nanopore in AAM contains copious unsaturated bonds, indicating that it may accept C clusters. The

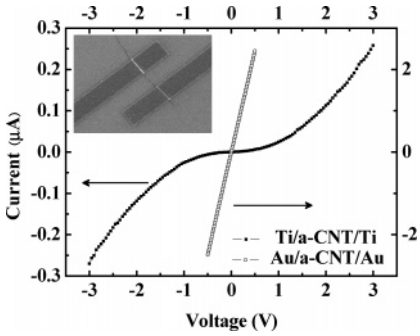

Figure 7. Room temperature $I-V$ characteristics of a-CNT-based devices. The inset is a SEM image showing a Au/a-CNT/Au device used in the experiment. The spacing between the Au electrodes is 2 μm.

finite carbon source confined in the nanochannels led to the ultrathin wall of the CNTs. The last liberated Fe atoms gathered to form large clusters by collision and diffusion and dwelled inside the tubes. The Fe clusters further reacted with the residue oxygen forming iron oxide nanoparticles, part of which were enwrapped by the amorphous carbon shell. The iron oxide nanoparticles were randomly distributed inside the nanotubes.

Step 4: The AAM was completely removed by etching in diluted NaOH solution or HCl solution. The resulting CNTs were monodisperse, rigid, and straight. The posttreatment at room temperature could not further oxidize the nanoparticles. We are convinced that the oxidization reaction occurred during the pyrolysis.

Ferrocene has been shown to be a good catalyst precursor or carbon source suitable for CNT growth.[19−23] When pyrolyzing pure ferrocene[21−23] at low temperature (below 700 °C), the main products were spherical Fe nanoparticles enwrapped by carbon material. No CNTs were obtained under these conditions. At high temperature (above 900 °C), a limited amount of nanotube material was found among the dominating spherical particles and irregular C−Fe mixture aggregations. But when ferrocene together with other hydrocarbon compounds were used,[19,20] high-quality CNTs were obtained. This result suggests that ferrocene is a good catalyst, which is determined by its pyrolysis properties. In our experiment ferrocene served mainly as a carbon source rather than catalyst precursor based on the above analyses. The AAM template provided a confined space and a special inner wall to favor the formation of the tubular structure, which was thus regarded as a catalysis effect.[24,25] The amorphous structure of the CNT was related to the decomposition temperature, which was not high enough to rearrange completely the C clusters into perfect concentric graphenes.

Nanoelectronic devices were fabricated by using the a-CNTs, and their electrical transport properties were measured at room temperature in a vacuum chamber.[26] Au and Ti/Au were selected as the electrode materials because of their different work function and contacting behavior with CNTs. The current−voltage ($I-V$) characteristic for both cases was plotted in Figure 7. The inset in Figure 7 shows a SEM image of a device with the a-CNT symmetrically contacted with Au electrodes. In the case of Au electrodes, it was found that the $I-V$ curve is linear, illustrating a good ohmic behavior while for the case of Ti/Au electrodes, the $I-V$ curve displays a clear Schottky contact behavior. The different work function of the electrodes (Au: 5.1 eV; Ti: 4.33 eV) leads to distinct contact behavior, suggesting that the transport properties of the device may be controlled by selecting the appropriate metal with the desired work function. In the case of Au electrodes, the resistivity of the a-CNT may be estimated from the linear $I-V$ curve to be 4.5×10^{-3} Ω cm, which is of the same order as a multiwalled CNT.[27] Since the a-CNT forms ohmic contact with Au, the estimated resistivity is not expected to be affected very much by the contact resistance. On the other hand, for the Schottky contact with Ti, the contact resistance may play a larger role and become not negligible. The metal particles encapsulated in the CNTs as shown in Figure 4 are also expected to affect the transport of the a-CNT. However, these metal particles may be removed from the nanotubes and their effect on the $I-V$ curve may be eliminated by passing a large current through the nanotube as a result of the electromigration effect.[28,29]

4. Conclusions

In summary, we demonstrated that a simple fabrication procedure may be used for preparing highly ordered carbon nanotube arrays. This approach involves the sublimation of ferrocene into the nanopores and pyrolysis of the confined ferrocene within nanopores of the AAM template. SEM, TEM, EDS, EELS, and Raman analyses show that the nanotubes hold ultrathin amorphous wall (∼3 nm) and some iron oxide nanoparticles are encapsulated within the nanotubes. The a-CNT growth results mainly from the pyrolysis of ferrocene confined within the nanoscale pores of the AAM. The electrical transport measurement on individual a-CNTs reveals that their resistivity is of the same order as the well-graphitizied multiwalled CNTs despite their disordered microstructure. The electrical contacts may be made either ohmic or Schottky type depending on the properties of the electrode materials. The highly ordered and densely packed a-CNT arrays with ultrathin wall are expected to find applications, among other things, as field emitters, nanoelectronic devices, catalyst supports, and energy conversion and storage materials.

Acknowledgment. This work is supported by the Ministry of Science and Technology (973 Grant No. 001CB610502, 863 Grant No. 2004AA302G11), National Science Foundation of China (Grant Nos. 90206201 and 10434010), the Chinese Ministry of Education (Key Project, Grant No. 10401), and the National Center for Nanoscience and Technology of China.

References and Notes

(1) Iijima, S. *Nature* **1991**, *354*, 56.
(2) Dresselhaus, M. S.; Dresselhaus, G.; Avouris, Ph. *Carbon Nanotubes Synthesis, Structures, and Applications*; Springer: Berlin, Germany, 2001.
(3) Ebbesen, T. W.; Ajayan, P. M. *Nature* **1992**, *358*, 220.
(4) Thess, A.; Lee, R.; Nikolaev, P.; Dai, H. J.; Petit, P.; Robert, J.; Xu, C.; Lee, Y. H.; Kim, S. G.; Rinzler, A. G.; Colbert, D. T.; Scuseria, G. E.; Tomanek, D.; Fischer, J. E.; Smalley, R. E. *Science* **1996**, *273*, 483.
(5) Endo, M.; Takeuchi, K.; Igarashi, S.; Kobori, K.; Shiraishi, M.; Kroto, H. W. *J. Phys. Chem. Solids* **1993**, *54*, 1841.
(6) Charlier, J. C. *Acc. Chem. Res.* **2002**, *35*, 1063.
(7) Rakitin, A.; Papadopoulos, C.; Xu, J. M. *Phys. Rev. B* **2000**, *61*, 5793.
(8) Nishino, H.; Yamaguchi, C.; Nakaoka, H.; Nishida, R. *Carbon* **2003**, *41*, 2165.
(9) Ci, L. J.; Wei, B. Q.; Xu, C. L.; Liang, J.; Wu, D. H.; Xie, S. S.; Zhou, W. Y.; Li, Y. B.; Liu, Z. Q.; Tang, D. S. *J. Cryst. Growth* **2001**, *233*, 823.
(10) Lu, A. H.; Schmidt, W.; Tatar, S. D.; Spliethoff, B.; Popp, J.; Kiefer, W.; Schüth, F. *Carbon* **2005**, *43*, 1811.
(11) Xiong, Y. J.; Xie, Y.; Li, X. X.; Li, Z. Q. *Carbon* **2004**, *42*, 1447.
(12) Li, J.; Papadopoulos, C.; Xu, J. M.; Moskovits, M. *Appl. Phys. Lett.* **1999**, *75*, 367.
(13) Kyotani, T.; Tsai, L. F.; Tomita, A. *Chem. Mater.* **1996**, *8*, 2109.
(14) Hu, Z. D.; Chen, Q.; Peng, L.-M. Submitted for publication.
(15) Masuda, H.; Fukuda, K. *Science* **1995**, *268*, 1466.
(16) Ferrari, A. C.; Robertson, J. *Phys. Rev. B* **2000**, *61*, 14095.
(17) Martin, C. R. *Science* **1994**, *266*, 1961.
(18) Elihn, K.; Larsson, K. *Thin Solid Films* **2004**, *458*, 325.

(19) Zhu, H. W.; Xu, C. L.; Wu, D. H.; Wei, B. Q.; Vajtai, R.; Ajayan, P. M. *Science* **2002**, *296*, 884.

(20) Wei, B. Q.; Vajtai, R.; Jung, Y.; Ward, J.; Zhang, R.; Ramanath, G.; Ajayan, P. M. *Nature* **2002**, *416*, 495.

(21) Sen, R.; Govindaraj, A.; Rao, C. N. R. *Chem. Phys. Lett.* **1997**, *267*, 276.

(22) Sano, N.; Akazawa, H.; Kikuchi, T.; Kanki, T. *Carbon* **2003**, *41*, 2159.

(23) Hou, H. Q.; Schaper, A. K.; Weller, F.; Greiner, A. *Chem. Mater.* **2002**, *14*, 3990.

(24) Jeong, S. H.; Hwang, H. Y.; Hwang, S. K.; Lee, K. H. *Carbon* **2004**, *42*, 2073.

(25) Lee, J. S.; Gu, G. H.; Kim, H.; Jeong, K. S.; Bae, J.; Suh, J. S. *Chem. Mater.* **2001**, *13*, 2387.

(26) Hu, Y. F.; Liang, X. L.; Chen, Q.; Peng, L.-M.; Hu, Z. D. *Appl. Phys. Lett.* **2006**, *88*, 063113.

(27) Wei, B. Q.; Spolenak, R.; Philipp, K. R.; Manfred, R.; Eduard, A. *Appl. Phys. Lett.* **1999**, *74*, 3149.

(28) Sorbello, R. S. *Solid State Phys.* **1998**, *51*, 159.

(29) Jin, C. H.; Wang, J. Y.; Chen, Q.; Peng, L.-M. *J. Phys. Chem. B* **2006** in press.